Universidad de Cantabria

Facultad de Ciencias

ON LIGHT SCATTERING BY NANOPARTICLES WITH CONVENTIONAL AND NON-CONVENTIONAL OPTICAL PROPERTIES

PH.D. THESIS

Braulio García-Cámara

Santander, July 2010

Part II

Study of the Scattering Properties of Agglomerates of Nanoparticles

6

Dimers of Nanoparticles with Directional Behaviors: Far- and Near-Field Calculations

"Ningún grupo puede actuar con eficacia si falta el concierto; ningún grupo puede actuar en concierto si falta la confianza"
—Edmund Burke, 1729-1797, escritor y pensador político británico

6.1. Introduction

Until now we have spent a considerable amount of time studying the light scattering properties of an isolated particle with electric and magnetic properties, and more specifically in the double-negative range. This, as we have shown, opens the possibility to manipulate the directionality of light scattering by tuning the values of ϵ and μ.

In the last years, studies about coupling interactions between nanoparticles or nanorods have proliferated, either from a theoretical [95, 94, 44, 31, 80] or an experimental [43, 110, 74] point of view. In all of these cases, interactions between nanoparticles produce appreciable effects, modifying the spectral scattering properties of the isolated nanoparticles.

Motivated by these and other studies, this chapter is devoted to the study of the interaction between small particles with optical constants in the non-conventional range ($\epsilon < 0$ or $\epsilon > 0$ and $\mu \neq 1$) and presenting directional scattering properties, which we will call here directionality. The scattering diagrams of dimers with these non-conventional optical properties are analyzed in order to evaluate the influence of the directional properties of each particle and their interactions on the overall scattering angular distribution. These effects have been studied both in the far-field and the near-field range.

In the far-field range and considering large inter-particle distances (larger than R), the assumption that consists to consider each component of the aggregate as a dipole is accurate and the CEMDM (Coupled Electric and Magnetic Dipole Method) [105] can be used. On the other hand, in the near-field, the size effects and the multipolar contributions become important and the dipolar approximation cannot be applied anymore [21, 36]. For distances comparable to the particle size, several methods based on differential equations formulation, such as the finite difference time domain (FDTD) [150, 35, 27], finite element methods (FEM) [101], or on integral equations, as the extinction's theorem [84, 137], are adequate to analyze the interaction of electromagnetic radiation with matter. In this particular case, we have used a computational method based on surface integral equations (SIE). The computational tool was developed by Andreas Kern and Prof. Olivier Martin [70] from the Nanophotonics and Metrology Laboratory of the École Polytechnique Fédérale de Lausanne (EPFL), with whom we have collaborated.

6.2. Coupled Electric and Magnetic Dipole Method

Light scattering by an ensemble of interacting nanoparticles with electric and magnetic properties was described, in detail, several years ago by G. Mulholland, C. Bohren and K. Fuller [105]. In their work, the authors introduced the so-called Coupled Electric Dipole Method (*CEDM*) developed by S. Singham *et al.* [127]. This method considers each particle forming the aggregate as a simple electric dipole described by an electric dipolar moment ($\overrightarrow{p}$). G. Mulholland and co-authors went a step forward generalizing it for particles with electric and also magnetic response to an incident electromagnetic field. In this new method, which they called Coupled Electric and Magnetic Dipole Method (CEMDM), particles are represented with an electric ($\overrightarrow{p}$) and a magnetic ($\overrightarrow{m}$) dipole moment, as explained below. This method has been again analyzed, recently, by P. Chaumet and A. Rahmani using tensors for its formulation [20].

The *CEMDM* considers a system that is formed by *N* very small particles located at spatial points $\overrightarrow{r}_1, \overrightarrow{r}_2 ... \overrightarrow{r}_N$ and illuminated by an incident plane wave described by an electric and magnetic field as

$$\overrightarrow{E}_0^i = E_0 e^{i\vec{k}_0\vec{r}_i} \tag{6.1}$$

$$\overrightarrow{H}_0^i = H_0 e^{i\vec{k}_0\vec{r}_i} \tag{6.2}$$

where $\vec{E}_0^i$ and $\vec{H}_0^i$ are the local electric and magnetic fields, respectively, at the point $\overrightarrow{r}_i$ and $\overrightarrow{k}_0$ is the wavevector of the incident field. Each component of the system is considered much smaller than the incident wavelength (λ), for this reason, it is possible to describe each of them as dipoles through their dipolar moments (see section 5.2). While for an isolated particle (see section 5.2) the electromagnetic field that is introduced in the expressions of the dipolar moments is the incident plane wave, when we consider an aggregate of particles, the local field on each of them is the sum of the incident field (equations 6.1 and 6.2) and the fields scattered by the rest of the particles. Mulholland et al [105] described, mathematically, the contributions to the electric and magnetic field at the *ith* particle due to the other constituents, represented, as well, by their electric and magnetic dipole moments, as

$$\overrightarrow{E}_i = \sum_{j\neq i}^{N} a_{ij}\alpha_E \overrightarrow{E}_j + b_{ij}\alpha_E \left(\overrightarrow{E}_j \cdot \overrightarrow{n}_{ji}\right)\overrightarrow{n}_{ji} - d_{ij}\left(\frac{\mu_0}{\epsilon_0}\right)^{1/2}\alpha_H\left(\overrightarrow{n}_{ji} \times \overrightarrow{H}_j\right) \tag{6.3}$$

$$\overrightarrow{H}_i = \sum_{j\neq i}^{N} a_{ij}\alpha_H \overrightarrow{H}_j + b_{ij}\alpha_H \left(\overrightarrow{H}_j \cdot \overrightarrow{n}_{ji}\right)\overrightarrow{n}_{ji} + d_{ij}\left(\frac{\epsilon_0}{\mu_0}\right)^{1/2}\alpha_E\left(\overrightarrow{n}_{ji} \times \overrightarrow{E}_j\right) \tag{6.4}$$

where $\overrightarrow{n}_{ji}$ is the direction vector from the *jth* particle to the *ith* one. The coefficients a_{ij}, b_{ij} and d_{ij} are given by

$$a_{ij} = \frac{1}{4\pi}\frac{e^{ik_{ij}^r}}{r_{ij}}\left(k^2 - \frac{1}{r_{ij}^2} + \frac{ik}{r_{ij}}\right) \tag{6.5}$$

$$b_{ij} = \frac{1}{4\pi}\frac{e^{ik_{ij}^r}}{r_{ij}}\left(-k^2 + \frac{3}{r_{ij}^2} - \frac{3ik}{r_{ij}}\right) \tag{6.6}$$

$$d_{ij} = \frac{1}{4\pi}\frac{e^{ik r_{ij}}}{r_{ij}}\left(k^2 + \frac{ik}{r_{ij}}\right) \tag{6.7}$$

r_{ij} being the distance between the two considered particles (*i* and *j*) and *k* is the wave number ($k = 2\pi/\lambda$).

As can be seen, the previous equations are coupled and the use of matrices is very convenient to solve the local fields. Thereto we define the following matrices:

$$\mathbf{C_{ij}} = \begin{pmatrix} a_{ij} + b_{ij}(n_{ji}^x)^2 & b_{ij} n_{ji}^x n_{ji}^y & b_{ij} n_{ji}^x n_{ji}^z \\ b_{ij} n_{ji}^y n_{ji}^x & a_{ij} + b_{ij}(n_{ji}^y)^2 & b_{ij} n_{ji}^y n_{ji}^z \\ b_{ij} n_{ji}^z n_{ji}^x & b_{ij} n_{ji}^z n_{ji}^y & a_{ij} + b_{ij}(n_{ji}^z)^2 \end{pmatrix} \tag{6.8}$$

$$\mathbf{f_{ij}} = \begin{pmatrix} 0 & -d_{ij} n_{ji}^z & d_{ij} n_{ji}^y \\ d_{ij} n_{ji}^z & 0 & -d_{ij} n_{ji}^x \\ -d_{ij} n_{ji}^y & d_{ij} n_{ji}^x & 0 \end{pmatrix} \tag{6.9}$$

Then, the total field on the *ith* particle, is the sum of the incident plane wave and the field defined in equations (6.3) and (6.4) and can be written as

$$\overrightarrow{E}_i^t = \overrightarrow{E}_0 + \alpha_E \sum_{j \neq i}^{N} C_{ij} \overrightarrow{E}_j + \alpha_H \sum_{j \neq i}^{N} f_{ij} \overrightarrow{H}_j \tag{6.10}$$

$$\overrightarrow{H}_i^t = \overrightarrow{H}_0 + \alpha_H \sum_{j \neq i}^{N} C_{ij} \overrightarrow{H}_j + \alpha_E \sum_{j \neq i}^{N} f_{ij} \overrightarrow{E}_j \tag{6.11}$$

or in a more condensed form

$$\begin{pmatrix} \overrightarrow{E}_i^t \\ \overrightarrow{H}_i^t \end{pmatrix} = \begin{pmatrix} \overrightarrow{E}_0 \\ \overrightarrow{H}_0 \end{pmatrix} + \begin{pmatrix} \alpha_E C_i & \alpha_H f_i \\ \alpha_E f_i & \alpha_H C_i \end{pmatrix} \begin{pmatrix} \overrightarrow{E}_i^t \\ \overrightarrow{H}_i^t \end{pmatrix} = \begin{pmatrix} \overrightarrow{E}_0 \\ \overrightarrow{H}_0 \end{pmatrix} + G \begin{pmatrix} \overrightarrow{E}_i^t \\ \overrightarrow{H}_i^t \end{pmatrix} \tag{6.12}$$

From this expression, it is easy to obtain the total field at the position of the *ith* subunit by a simple matrix inversion

$$(I - G) \begin{pmatrix} \overrightarrow{E}_i^t \\ \overrightarrow{H}_i^t \end{pmatrix} = \begin{pmatrix} \overrightarrow{E}_0 \\ \overrightarrow{H}_0 \end{pmatrix} \begin{pmatrix} \overrightarrow{E}_i^t \\ \overrightarrow{H}_i^t \end{pmatrix} = (I - G)^{-1} \begin{pmatrix} \overrightarrow{E}_0 \\ \overrightarrow{H}_0 \end{pmatrix} \tag{6.13}$$

Finally, the last equation (6.13) corresponds to the local electromagnetic field at the *ith*

particle (being the sum of the incident plane wave and the contributions from the other particles forming the aggregate). These electric and magnetic fields, can be introduced in equations (5.5) and (5.6) to obtain the dipolar moments describing this nanoparticle. Once we have the corresponding dipolar moments, the scattered field of the aggregate can be calculated as a simple phase sum of the scattered field by each particle which can be directly deduced using expressions (5.1), (5.3), (5.2) and (5.4), described in a previous chapter and obtained from [105] or [57].

6.3. Surface Integral Equations for 3D Nanostructures

Although the calculations and the development of the numerical method has been made by the group of O. Martin, a few lines about the method are included. For a complete explanation of the theory and the numerical methods used, see the reference [70].

The Surface Integral Equation (SIE) method solves Maxwell's equations using dyadic Green's functions $\overline{\mathbf{G}}_i$. The main advantage of this is the reduction in memory with respect to other equivalent methods. This reduction is obtained by: i) rewriting the volumen integral equations (VIE) to a surface problem (SIE) which involves a scaling with the second power of the dimensions instead of a third power and ii) the fact that only the scatterer should be discretized, unlike in others methods where both the scatterer and the surrounding medium must be meshed [70]. In this particular case we use a complementary method known as Method of Moments (MoM) [49] to determine the integral equation (IE), appearing during the solution of the problem, on the meshed surface of the scatterers.

6.4. Far-Field Light Scattering of a Dimer of Nanoparticles with Unconventional Optical Properties

This section has been devoted to analyze the scattering diagrams of aggregates of nanoparticles with similar size and optical constants such that each particle presents directional behaviors. The main objective of this study is to extend the former analysis to clusters of nanoparticles testing the influence of possible interactions between particles in the overall angular distribution of light scattering in far-field.

In general, one could consider *N* particles at positions $\overrightarrow{r}_1, \overrightarrow{r}_2, ..., \overrightarrow{r}_N$ given in spherical

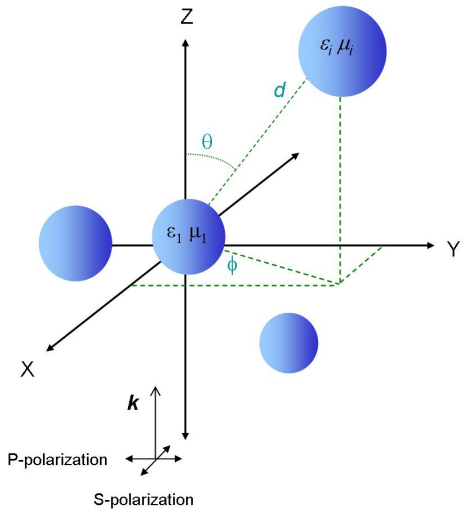

Figure 6.1: Schematic representation of an aggregate made of nanoparticles with radius *R* and different optical constants (ϵ_i, μ_i) illuminated by a plane wave in the z-direction and linearly polarized. Particle positions are fixed using spherical coordinates.

coordinates as is shown in Figure 6.1. However, for time and space requirements, we have chosen the simplest aggregate in which multiple scattering is present, a dimer, composed of two particles with the same size. The optical constants are chosen such that both of them do not scatter either in the forward or in the backward direction for different separation distances and alignments. Also, a combining dimer, which will be explained later, is analyzed.

The method used to calculate the scattering patterns are based on the dipolar approximation, as was explained above. For this reason, the distances between particles are considered large enough to reduce strong interactions and multipolar effects.

Three particular cases are shown in this chapter: when both particles present optical constants such that light scattering in the forward direction is minimum, when (ϵ, μ) of both produce a minimum in the backward direction and finally when one particle has a minimum forward scattering and the other one a minimum backward scattering. This last case is what we will call the combined configuration.

6.4.1. Particles with Minimum Forward Scattering

A pair of particles with a radius $R = 0.01\lambda$ separated by a distance d and aligned parallel to one of the main axis (*X, Y or Z*) is considered. The optical constants of both particles are chosen such that they fulfill the zero-forward condition proposed by Kerker et al. [69]. Although, along this thesis we have focused on the double-negative (DNG) range, in this

particular study we have considered double-positive values. However, similar calculations were made in the DNG range with similar results.

Figure 6.2 shows the scattering patterns of two isolated particles, presenting a minimum forward scattering $(\epsilon, \mu) = (3, 0.14)$. Several gap sizes are considered, all of them large enough to ensure that the CEMDM can be applied. In addition, the influence of the alignment of the dimer is studied by placing the dimer parallel to each main axis which corresponds to each row of Figure 6.2. Finally, the two different polarizations: incident electric field parallel (Figure 6.2 right column) or perpendicular (Figure 6.2 right column) to the scattering plane, are considered.

Some important conclusions can be drawn from these results. First, since each particle has optical constants satisfying the zero-forward condition, it is obvious that a minimum in the scattered intensity in the same direction is observed for the aggregate. For small gap sizes ($d \leq 0.2\lambda$), the dimer has a behaviour like as an isolated particle with similar properties as those of each subunit, and its scattering patterns are similar to those of one isolated one (see Chapter 4): a pronounced minimum in the forward direction and independence on the incident polarization. For these small distances, the scattering diagrams are similar whatever the alignment of the dimer. On the contrary, when the gap size increases, interferential effects induce the appearance of lobes. The number of lobes increases as the gap increases. These effects on the scattering diagrams, do not affect light scattering in the forward direction, which remains minimum. Even the angular range at which the scattered intensity is minimum is the same and the polarization independence persists for high gap sizes. When the particles's separation becomes important and interferential effects start to appear, the alignment of the particles with respect to the incident beam and the scattering plane acquires also importance. In this way, when particles are on the scattering plane, either parallel or perpendicular to the incident direction, new lobes in the scattering due to these interferences, appear. However, if both particles are located perpendicular to the scattering plane and parallel to the x-axis, scattered fields from each particle interfere constructively at every scattering angle, then no lobes appear, as can be seen in the last row of Figure 6.2.

In summary, a cluster of particles can show the same directional effects as their constituents if distances between them ensure weak interactions, as was expected. If we consider shorter distances and therefore stronger interactions and multipolar effects, other computational methods should be used.

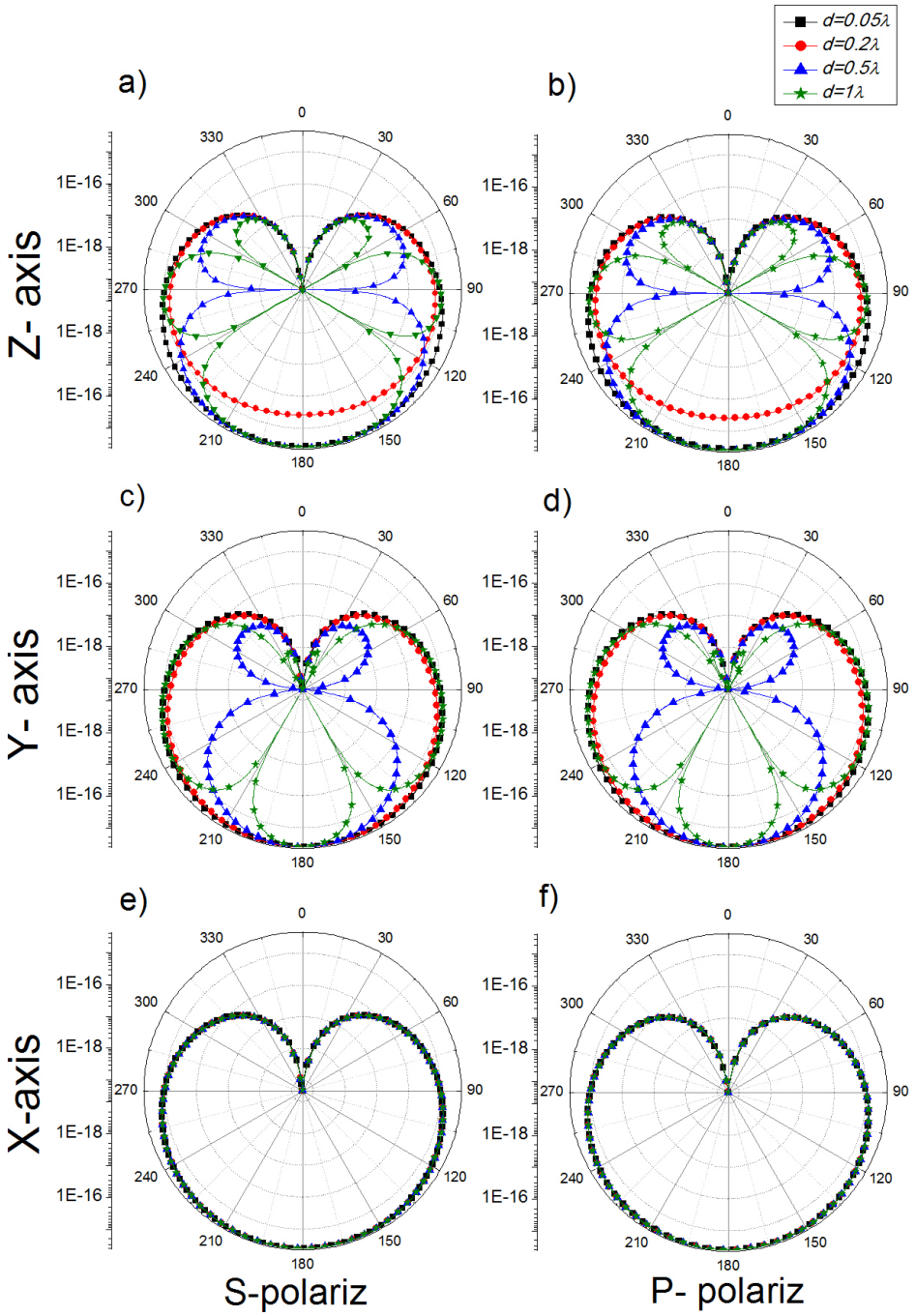

Figure 6.2: Scattering diagrams corresponding to a dimer of nanoparticles ($R = 0.01\lambda$) and optical constants fulfilling the zero-forward condition [69] $(\epsilon, \mu) = (3, 0.14)$ are plotted for several distances (d). The dimer is aligned following the three main axis (the corresponding axis is labeled on the left) and is illuminated by a plane wave, linearly polarized, and propagation parallel to the z-axis. Both polarizations are considered with the electric field parallel (right column) or perpendicular (left column) to the scattering plane

6.4.2. Particles with Minimum Backward Scattering

Similar results for particles under the zero-forward condition can be shown for particles which optical constants satisfying the zero-backward condition [69]. In Figure 6.3, the scattering diagrams for a dimer with the same geometrical conditions as the previous case and optical constants $(\epsilon, \mu) = (3, 3)$ for each subunit, are plotted. As can be seen, the behavior is quite similar to the minimum-forward case. Because of this similarity we do not repeat the whole analysis here.

6.4.3. Combined Configuration: Particles with Different Optical Constants

Here, the dimer is composed by two nanoparticles with a radius *R* and optical constants such that one of the components does not scatter in the forward direction and the other one does not scatter in the backward direction. This configuration is especially attractive when particles are aligned parallel to the incident direction and for this reason, only this orientation is considered. Depending on the placement of the particles, we can obtain a system in which each subunit scatters mainly to the dimer gap or to the exterior of the gap. We have called these configurations *gap* and *anti-gap* configurations, respectively (see Figure 6.4).

For our calculations, we take one of the particles with $(\epsilon, \mu) = (3, 0.14)$, having a minimum in the forward scattered intensity, and the other subunit with $(\epsilon, \mu) = (3, 3)$, presenting a minimum in the backward direction. Figure 6.5(a) and (b) summarize the scattering diagrams for the dimer under the gap-configuration (Figure 6.4 (a)), for several separation distances and both incident polarizations, perpendicular and parallel to the scattering plane, respectively. In addition, for comparison, scattering patterns for a dimer under identical geometrical conditions but with conventional optical constants ($\epsilon = 3, \mu = 1$), are shown in Figure 6.5 (c) and (d). As can be seen, in this case, the directionality of each component is completely hidden and the dimer with unconventional values of ϵ and μ, scatters in a similar way as the dimer made of dielectric particles. We can conclude that when both particles of the dimer present similar directionality, these can still be observed in the angular distribution of the scattered intensity by the dimer. However, when the dimer components present opposite directionalities, these can be canceled out and the dimer scatters as a conventional one. Similar results can be obtained for an anti-gap configuration but are not shown here.

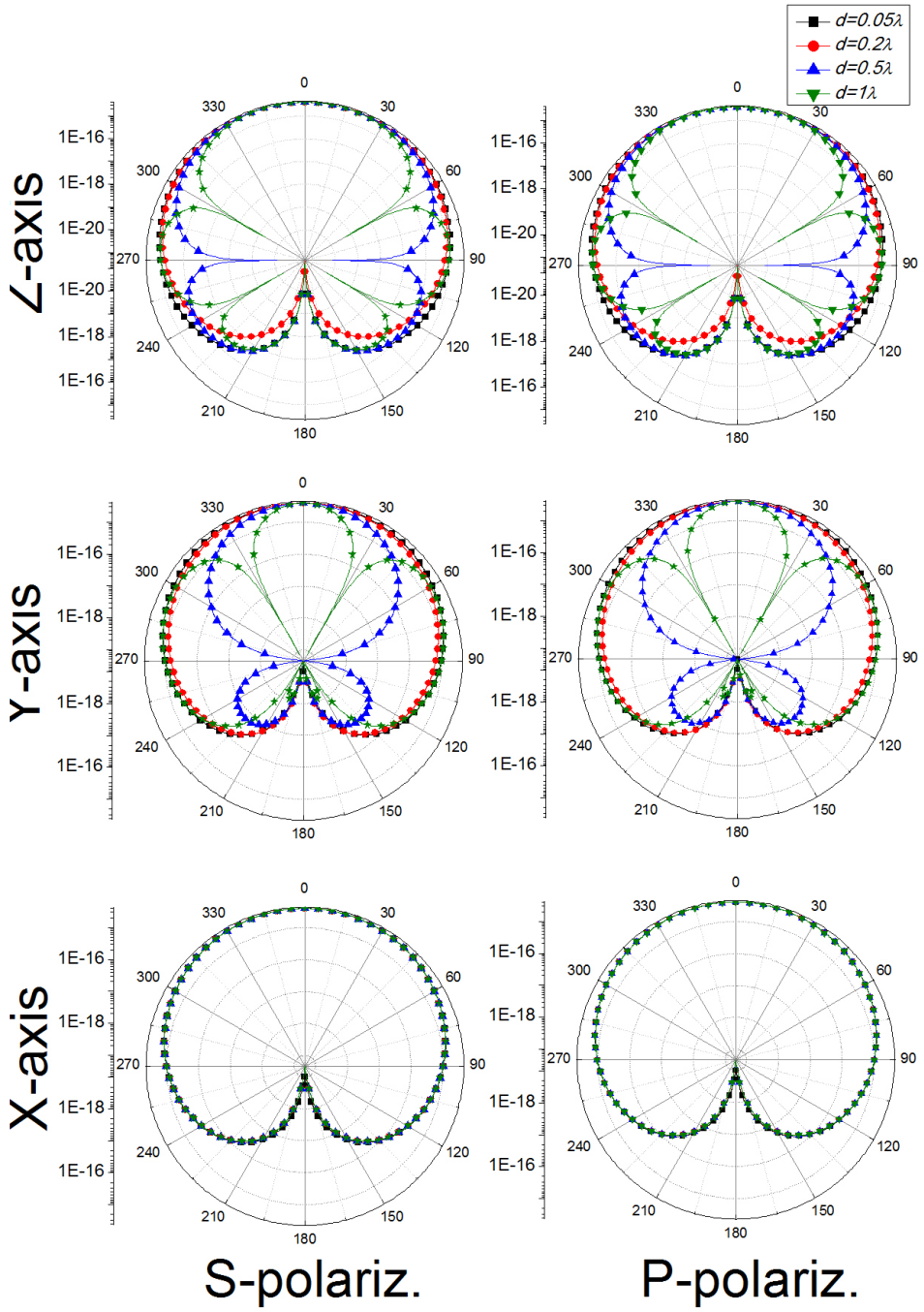

Figure 6.3: Scattering diagrams corresponding to a dimer of nanoparticles ($R = 0.01\lambda$) and optical constant fulfilling the zero-backward condition [69] $(\epsilon, \mu) = (3, 3)$ plotted for several separation distances (d). The dimer is aligned following the three main axis (the corresponding axis is labeled on the left) and is illuminated by a plane wave, linearly polarized, and propagating parallel to z-axis. Both polarizations are considered with the electric field parallel (right column) or perpendicular (left column) to the scattering plane

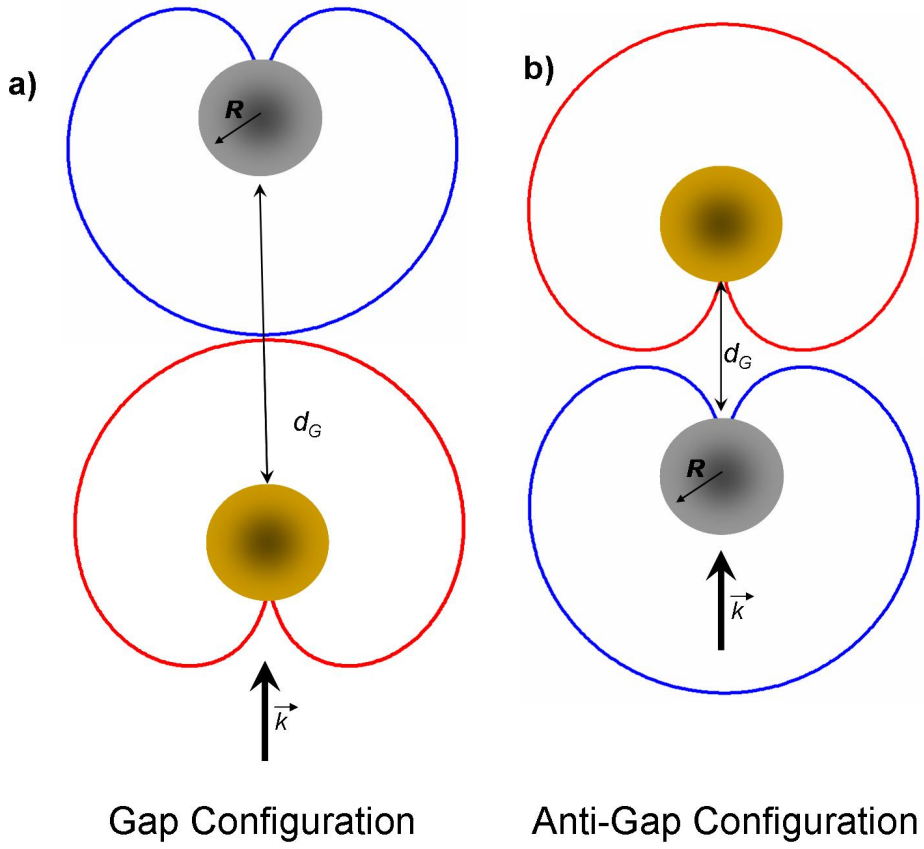

Figure 6.4: Schematic representation of a dimer composed of two nanoparticles of radius R, separated by a distance d_G and with optical constants $(\epsilon_1\mu_1)$ for the grey particle and (ϵ_2, μ_2) for the yellow one, satisfying the zero-backward and the zero-forward scattering conditions, respectively. The geometrical configurations are such that both particles scatter mainly to the gap (a) or in the opposite direction (b). In order to clarify these scattering distributions, the angular profile of the scattered intensity for each individual particle is also included.

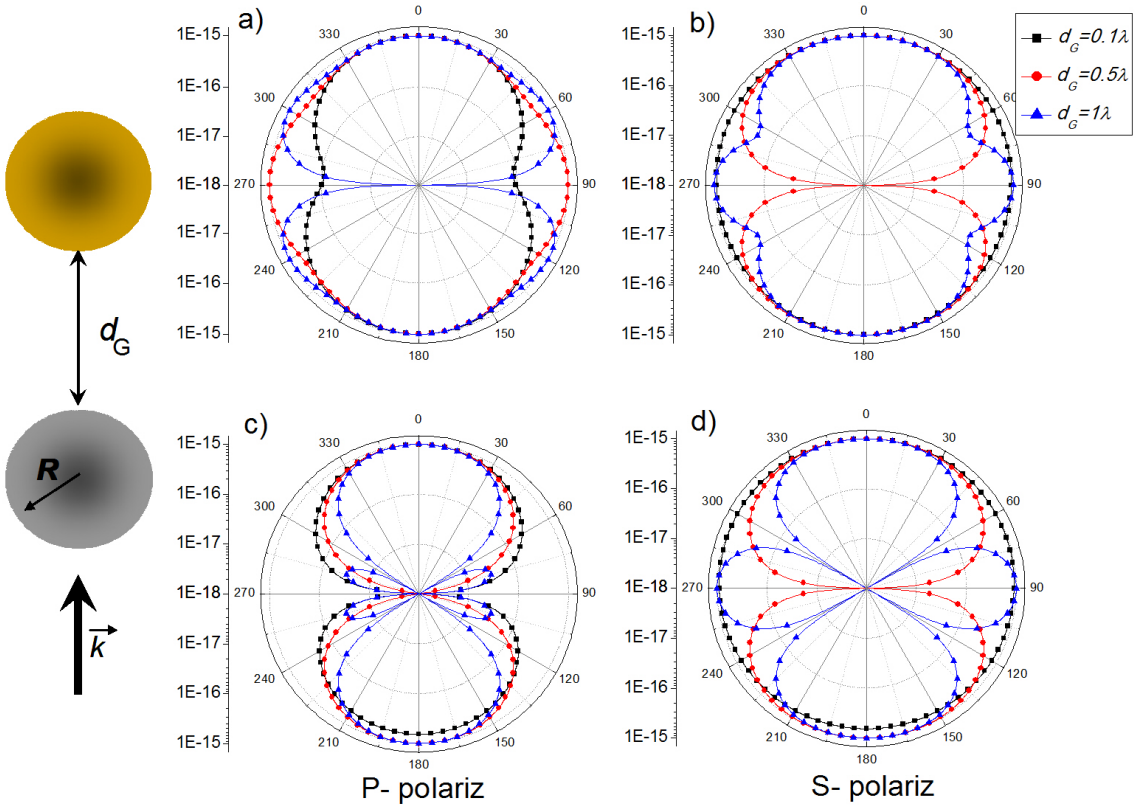

Figure 6.5: (a) and (b) Scattering diagrams of a dimer of nanoparticles ($R = 0.01\lambda$) when several separation distances, d, are considered. A basic scheme of the geometric conditions is included. The optical constants of each subunit are $(\epsilon, \mu) = (3, 0.14)$) for the top particle and $(\epsilon, \mu) = (3, 3)$ for the bottom one, which corresponds with the gap configuration. The dimer is located parallel to the incident linearly polarized beam. Both polarizations are considered with the electric field parallel (a) or perpendicular (b) to the scattering plane. For comparison, the scattering patterns for a dimer composed by dielectric particles $(\epsilon, \mu) = (3, 1)$ are also included in (c) and (d)

6.5. Near-field Light Scattering by a Dimer of Nanoparticles with Unconventional Optical Properties

In the previous section, the scattering patterns corresponding to an aggregate (dimer) of nanoparticles with unconventional values for the electric permittivity and the magnetic permeability were shown in the far-field region. As was shown, the directionalities of the isolated particles still followed the scattering diagrams of the aggregate, when aggregate components presented similar directionalities, although the particles were interacting. On the contrary, any directional behavior disappears if particles have opposite properties. This was shown when the observer is far from the cluster and separation distances, d_G, were also considered large enough to produce weak interactions and negligible multipolar effects.

One of the main potential applications of nanoparticles with directionality is the possibility to generate nanocircuits formed of these particles that would be able to lead light, following the idea proposed by N. Engheta in [32]. However, in those hypothetical circuits, the observation and separation distances would be quite smaller, that is in the near-field. For this reason, we have extended our analysis to the near-field light scattering by clusters of nanoparticles with directionality.

Time requirements obliged us to analyze only one configuration of those considered above. We choose the case in which each particle of a dimer present different optical constants in such a way that both components of the dimer scatter mainly to the gap (gap configuration, Figure 6.6) or in the opposite direction (anti-gap configuration, Figure 6.8). These could be very interesting to realize a very high and very low energy densities in the gap and anti-gap configurations respectively. The geometrical properties of these configurations are summarized in Figure 6.4. The grey particle has optical constants fulfilling a minimum-forward scattering $(\epsilon, \mu) = (-5 + 0.1i, -1 + 0.1i)$, while the optical properties of the yellow one satisfy a minimum-backward scattering $(\epsilon, \mu) = (-2.01 + 0.1i, -2.01 + 0.1i)$. Though a small absorption was included in the values of the permittivity and the permeability, its influence on the overall distribution is not important, qualitatively. Resonant features enhance strongly light scattering by this particle, which could enhance the transmitted signal through a circuit made of nanoparticles. For this reason, one of the particles, the yellow one, has been chosen with a double-resonance.

The proximity of the two particles could induce strong interactions of different nature, changing the distribution of the scattered intensity compared with the scattering pattern of

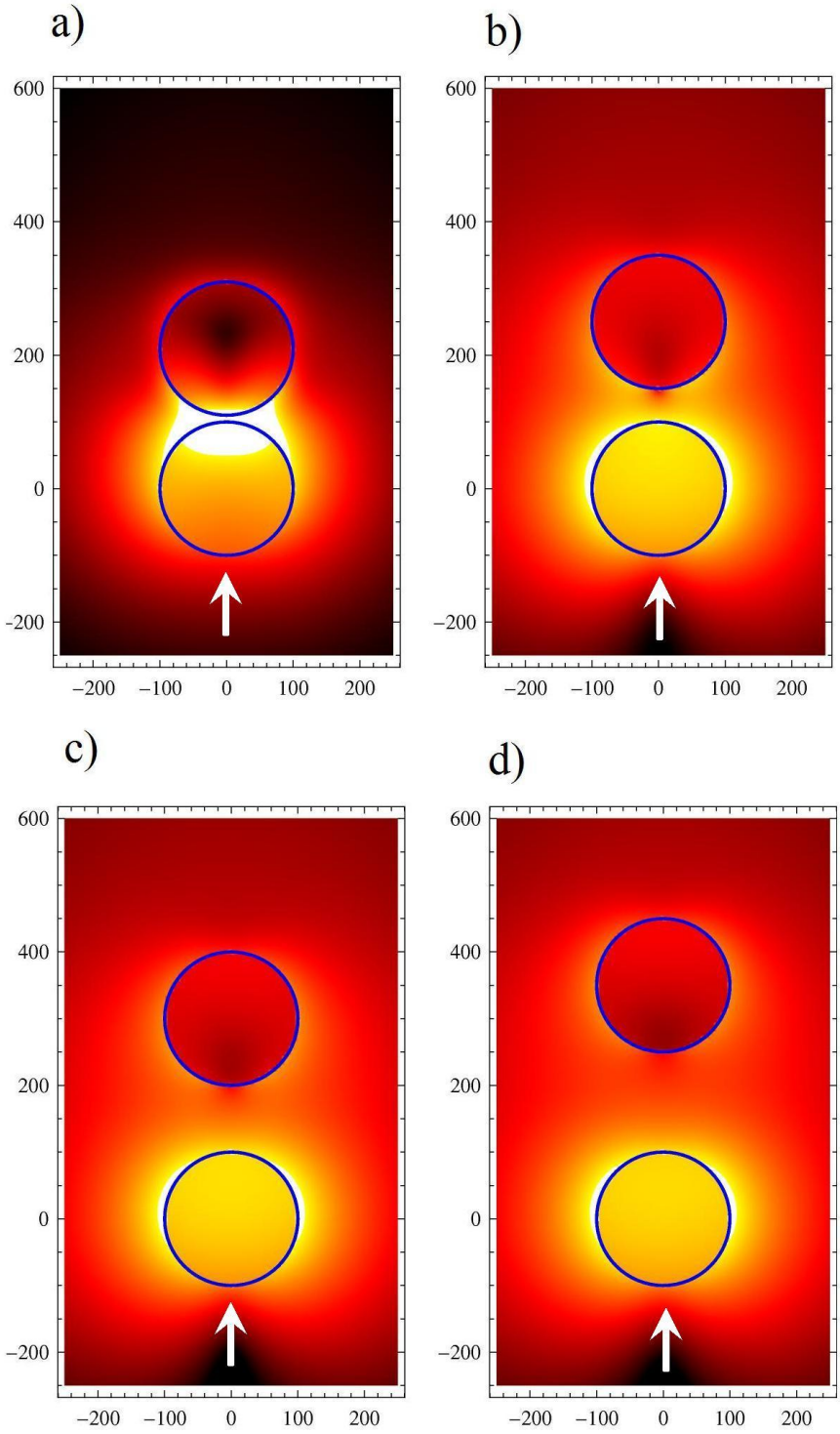

Figure 6.6: Distribution of the scattered intensity of a dimer of particles with a $R = 100nm$ (incident wavelength $\lambda = 1000nm$) and optical properties in such a way that they scatter mainly to the gap between them: the bottom one has $(\epsilon, \mu) = (-2.01 + 0.1i, -2.01 + 0.1i)$ while the top one is $(\epsilon, \mu) = -5 + 0.1i, -1 + 0.1i)$. The gap sizes are (a) $d_G = 0.1R$, (b) $d_G = 0.5R$, (c) $d_G = R$, (d) $d_G = 1.5R$. Bright colors mean high intensity while dark ones correspond to low scattered intensity. The spatial scale is in nanometers.

the isolated particle. As was stated by E. Hao and G. Schatz few years ago [48], for separation distances shorter than *R*, the interactions become strong. This was also observed in our calculations, as will be explained. However, in order to conserve partially the isolated behaviors, we have also considered larger distances but still comparable to the particle size.

For the purpose of comparing the results for directional particles, similar calculations using the method proposed by A. Kern and O.J.F. Martin, briefly explained previously [70], were made for two metallic particles with electric permittivities equal to that of our directional particles, that is $(\epsilon_1, \mu_1) = (-5+0.1i, 1)$ and $(\epsilon_2, \mu_2) = (-2.01+0.1i, 1)$. The spatial distribution of the scattered intensity by this metallic dimer is shown in Figure 6.7 where nanoparticles have a radius $R = 100nm$ and are illuminated by a plane wave with a wavelength $\lambda = 1000nm$ ($R = 0.1\lambda$) in the direction of the white arrow. The incident beam is linearly polarized with the electric field parallel to the scattering plane and several distances between particles are considered.

When the particles of our configurations are quite close, $d_G \sim 0.1R$ in Figure 6.7 (a), the strong interaction of scatterers hides the single particle behavior, showing high scattered intensities in the gap, as in [48]. For this reason, the spatial distribution for a dimer of metallic particles and for a dimer of particles with non-conventional optical constants, are quite similar as can be seen in panel (a) of Figures 6.7 (conventional case) and 6.6 (non-conventional case). The second case, the directional one, is such that the optical constants of the particles are: $(\epsilon, \mu) = (-2.01 + 0.1i, -2.01 + 0.1i)$ for the bottom particle and $(\epsilon, \mu) = (-5 + 0.1i, -1 + 0.1i)$ for the top one. While the bottom particle does not scatter in the backward direction, the top one does not scatter to the forward direction. This is the gap-configuration. As in the metallic case, for a directional configuration, the strong interaction at short distances obscured the directional features of each particle.

However, as the gap size increases, the interaction of particles becomes less strong and the footprint of the single particle starts to appear, in particular the directionality of non-conventional particles. Even for short distances, around a half of the particle radius ($d_G \sim 0.5R$), the differences between the directional (Figure 6.6 (b)) and the metallic case (Figure 6.7 (b)) become important. While in the second one, the scattered intensity in the gap starts to decrease and an important minimum appears on the surface of the top particle, this effect is minimized in the non-conventional case because particles tend to scatter in this direction increasing the scattered intensity in the gap. This effect can be observed better as the interaction between the particles decreases. For instance, for $d_G \sim R$, at which particles still interact but weakly [132], the differences between the conventional (Figure 6.7) and the non-conventional case (Figure 6.6) are obvious. While the directional configuration still

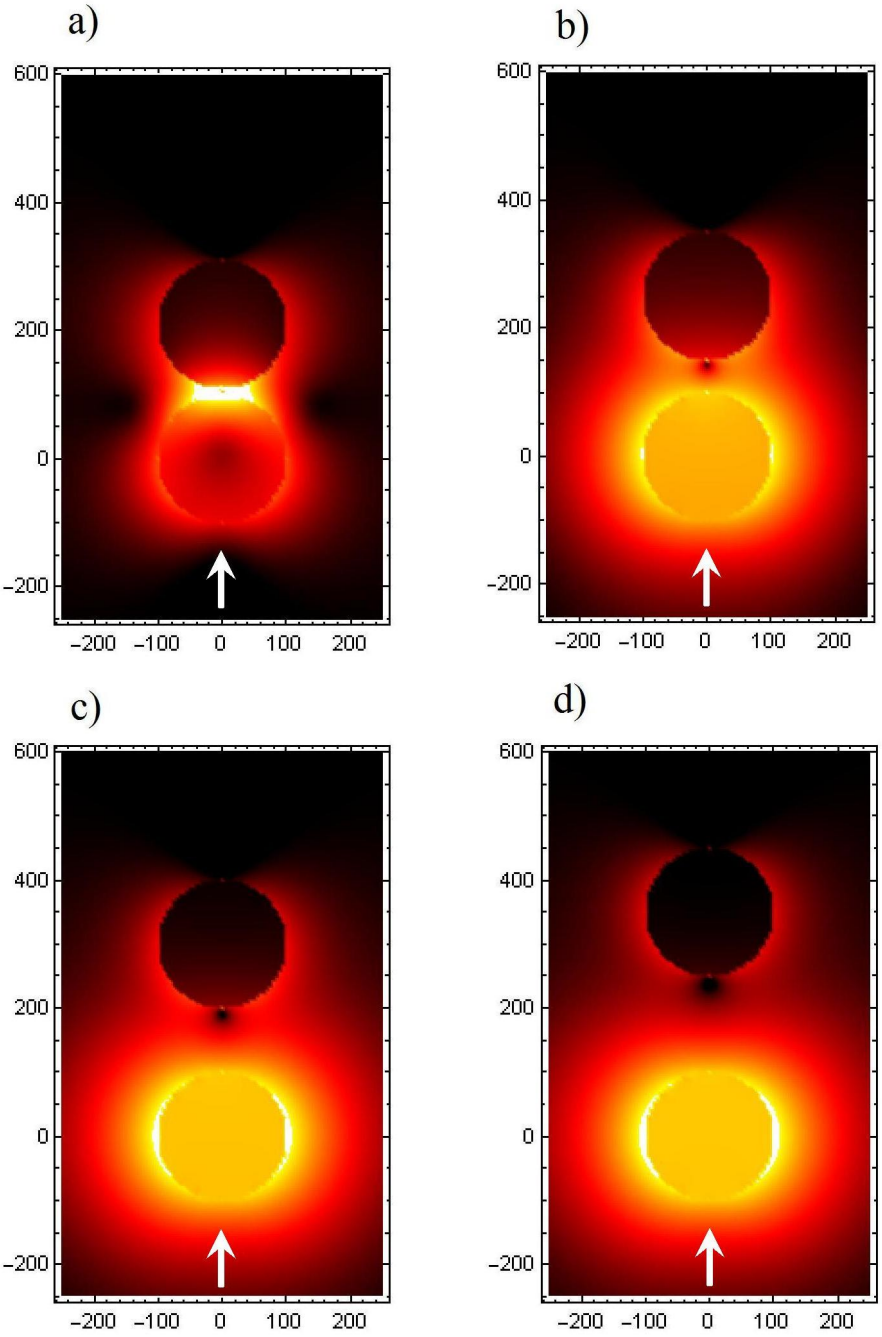

Figure 6.7: Conventional counterpart of Figure 6.6 where we plot the distribution of the scattered intensity of a dimer of particles with a $R = 100nm$ (incident wavelength $\lambda = 1000nm$) and optical properties in the metallic range: the bottom one has $(\epsilon, \mu) = (-2.01+0.1i, 1)$ while the top one has $(\epsilon, \mu) = (-5 + 0.1i, 1)$. The gap sizes are (a) $d_G = 0.1R$, (b) $d_G = 0.5R$, (c) $d_G = R$, (d) $d_G = 1.5R$. Bright colors mean high intensity while dark ones correspond to low scattered intensity. The spatial scale is in nanometers.

presents high scattered intensities in the gap between particles; when they are metallic, the scattered intensity in the gap is lower with a pronounced minimum (dark spot) on the surface of one of the particles. Going to the interaction limit ($d_G \sim 1.5R$), it is clearly seen that while metallic particles are completely uncoupled, with a spatial distribution of an electric dipole and small scattered intensities in the gap (Figure 6.7 (d)), the non-directional particles present their characteristic directionality with high intensities in the gap without any dark spot (Figure 6.6 (d)).

From these results, we can conclude that the directionality of particles with non-conventional values for ϵ and μ, are still observed in the near-field of aggregates consisting of such nanoparticles, when the interaction between those is not excessively strong. This could be useful for hypothetical nanocircuits or nanobiosensors in which one would be able to control the light distribution in the gap of dimers by tuning their optical constants. As we have induced a maximum distribution of the scattered intensity in the gap between the particles, we could produce a minimum, by interchanging the position of the particles. The results of this anti-gap configuration (Figure 6.4 (b)) are shown in Figure 6.8. In this case, contrary to the previous one, we are able to induce a sharp minimum in the center of the gap between the particles. This minimum is located in a different position from the one of the dark spot observed in Figure 6.7. While the minimum in the center of the gap in Figure 6.8 is generated by the combination of the scattering properties of each particle, the dark spot in the metallic case (Figure 6.9) is a consequence of the "eight-shape" of the scattered intensity by an electric dipole.

6.6. Conclusions

In this chapter, we have studied the distribution of the scattered intensity by dimers, composed of nanoparticles presenting directionality, as those presented in the previous part of this thesis. Several important parameters have been shown as being crucial: the observation distance, the inter-particle distance and the nature of the components.

First, we had to distinguish two important cases related with both the observation distance and the inter-particle distance. In the far-field region ($d \gg \lambda$), and for gap sizes large enough ($d_G > 2R$), the interaction between particles is weak and their internal structure can be neglected. A simple calculation method as the CEMDM can be used. However, for short distances, either between the cluster and the observer or between the constituents of the cluster, the interactions are more important and the appearance of higher orders than the

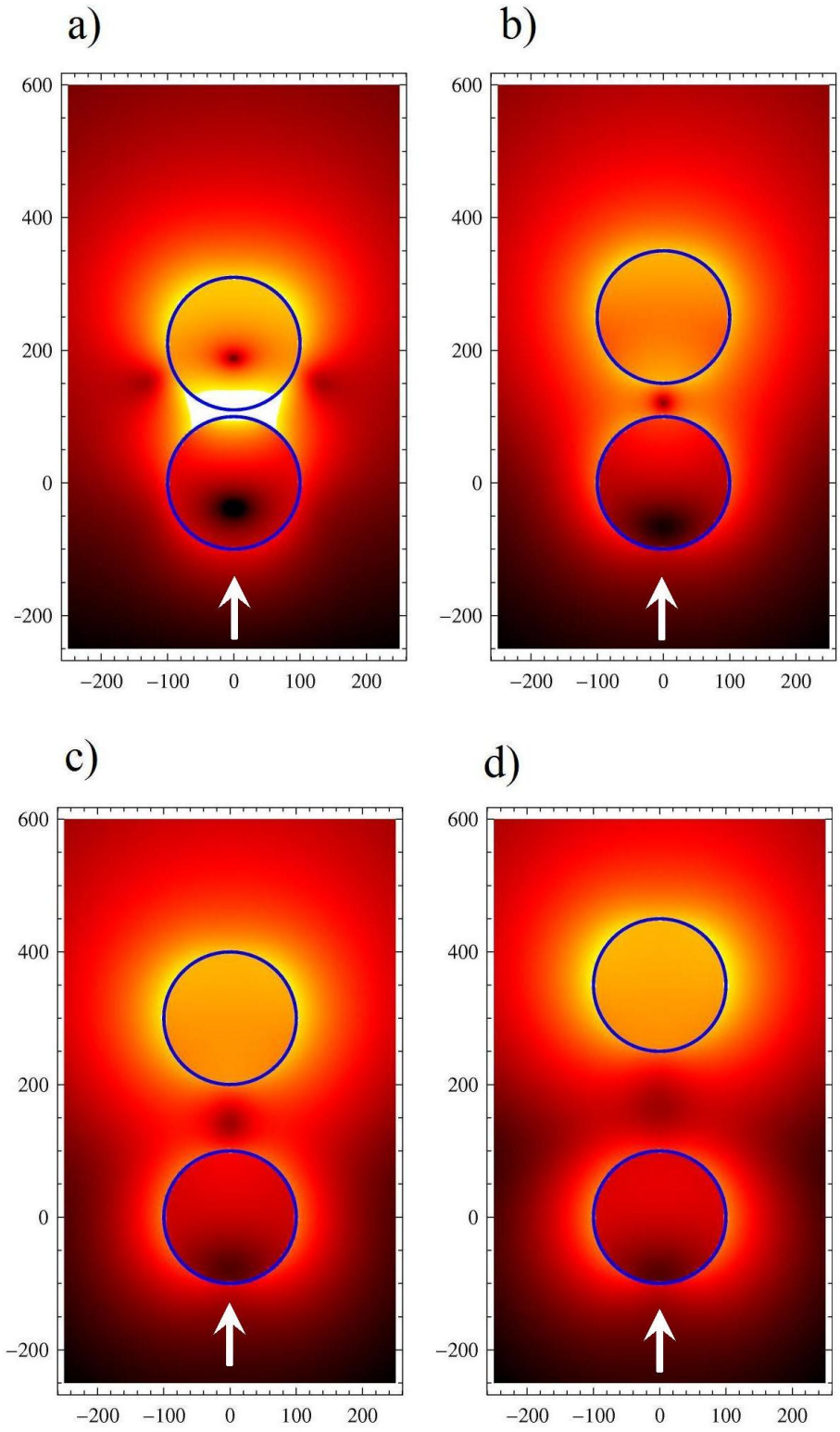

Figure 6.8: Distribution of the scattered intensity of a dimer of particles with a $R = 100nm$ (incident wavelength $\lambda = 1000nm$) and optical properties in such a way that they scatter mainly in the opposite direction of the gap: the bottom one has $(\epsilon, \mu) = (-5+0.1i, -1+0.1i)$ while the top one is $(\epsilon, \mu) = (-2.01 + 0.1i, -2.01 + 0.1i)$. As before, the gap sizes are (a) $d_G = 0.1R$, (b) $d_G = 0.5R$, (c) $d_G = R$, (d) $d_G = 1.5R$. Bright colors mean high intensity while dark ones correspond to low scattered intensity. The spatial scale is in nanometers.

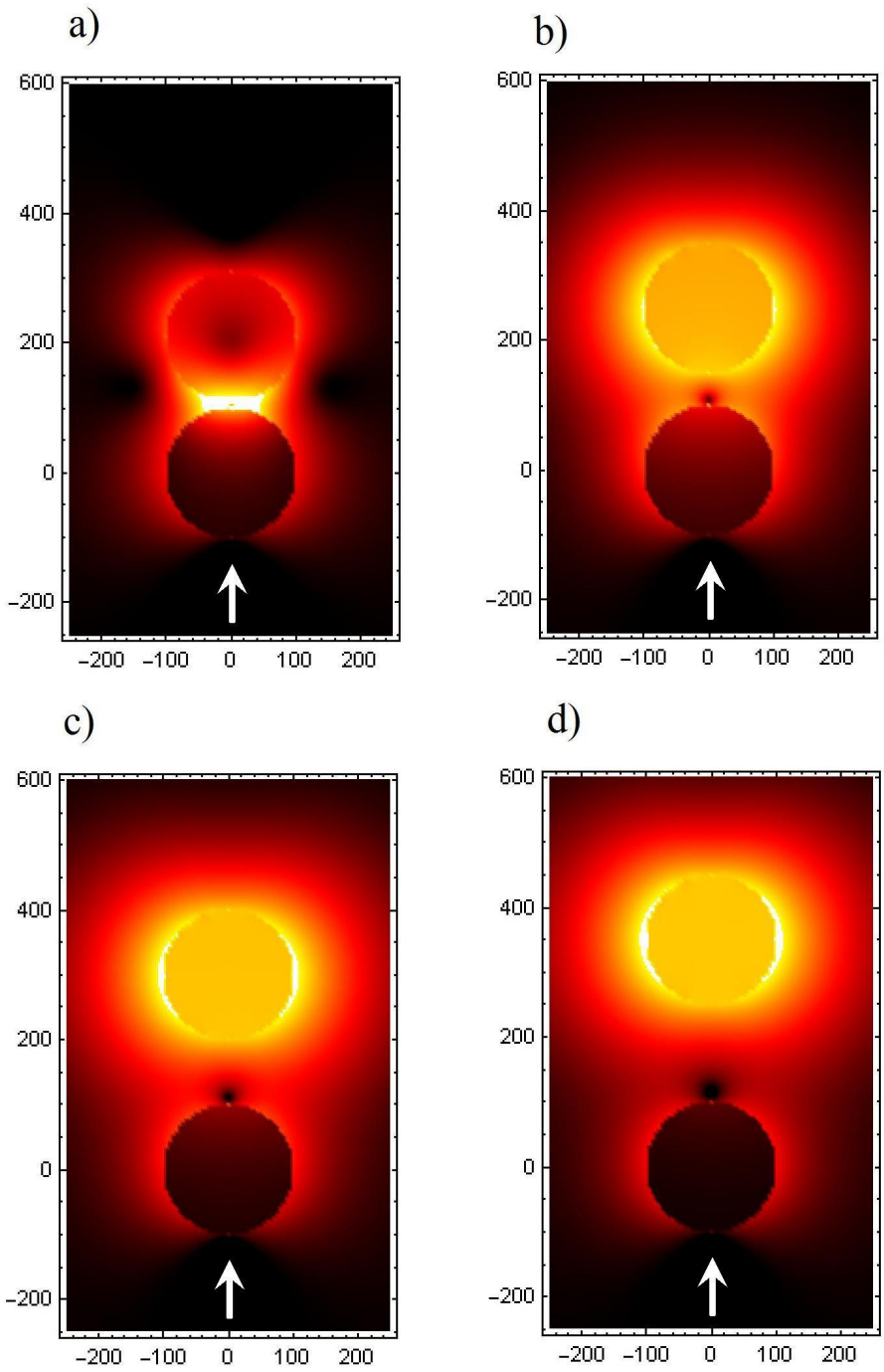

Figure 6.9: Conventional counterpart of Figure 6.8 where we plot the distribution of the scattered intensity of a dimer of particles with a $R = 100nm$ (incident wavelength $\lambda = 1000nm$) and optical properties in the metallic range: the bottom one has $(\epsilon, \mu) = (-5 + 0.1i, 1)$ while the top one is $(\epsilon, \mu) = (-2.01 + 0.1i, 1i)$. The gap sizes are (a) $d_G = 0.1R$, (b) $d_G = 0.5R$, (c) $d_G = R$, (d) $d_G = 1.5R$. Bright colors mean high intensity while dark ones correspond to low scattered intensity. The spatial scale is in nanometers.

dipolar one become more important. For this last situation, we have performed calculations based on surface integral equations (SIE) [70] in collaboration with O. Martin's group.

For long observation distances (far-field region) and with gap sizes larger than five times the radius of the particles, we showed that, when the constituents of the dimer have similar directionalities, that is, they present maxima or minima for the same scattering direction, the directionality also appears in the overall scattering patterns of the dimer. In addition, we have shown that this occurs for every type of alignment of the dimer and for several gap sizes. As the distance between particles increases, extra lobes appear in the scattering patterns due to interferential effects. Similar calculations with comparable results were carried out for trimers, although we do not show them here.

However, if the components of the dimer have opposite directional characters, in the so-called gap or anti-gap configuration, the angular distribution of the scattered intensity of the dimer does not present any directionality, being quite similar to that of a dimer formed of conventional particles. Nevertheless, these configurations, are quite interesting if we decrease both the observation and the inter-particle distances. After analyzing the results provided by A. Kern and O. Martin, we conclude that using configurations of nanoparticles as those described here, would offer the possibility to control the light distribution in the gap of a dimer. While for very small gap sizes the strong interaction between constituents hides any directionality, as distance slightly increases and the interaction decreases, directional features appear. For these gap sizes, we were able to obtain in our calculations maxima or minima in the center of the gap by tuning the optical constants of the particles.

In our opinion, these calculations could be useful for future designs of applications. The possibility to control the direction of light propagation through an ensemble of nanoparticles with previously chosen optical constants may lead to future optical communications on very small scales [50, 98].